Semiclassical theory of the hyperlens

Zubin Jacob, Leonid V. Alekseyev, and Evgenii Narimanov*

Department of Electrical Engineering, Princeton University, Princeton, New Jersey 08540, USA
**Corresponding author: evgenii@princeton.edu*

Received April 20, 2007; accepted May 15, 2007;
posted July 27, 2007 (Doc. ID 82286); published September 21, 2007

We study ray dynamics inside the hyperlens, a device capable of sub-diffraction-limited far-field imaging. An analytical result for the ray trajectories inside the hyperlens is obtained using Hamiltonian optics, which offers an alternative description of the device. It is also found that the ray trajectories can exhibit a unique spiraling nature inside the device. Numerical simulations of plane wave and Gaussian beam scattering from the hyperlens confirm the semiclassical description. © 2007 Optical Society of America

OCIS codes: 080.2720, 110.0180, 160.1190.

1. INTRODUCTION

Metamaterial technologies have paved the way for tailoring the dielectric [1], the magnetic [2,3], and even the mechanical response [4] of materials for interesting device applications. One such application, which has received much attention in recent times, is connected with overcoming the fundamental limitation of a conventional lens, which cannot form images with subwavelength resolution [5–7]. Beating this diffraction limit, which arises due to the loss of information carried by the evanescent waves emanating from an object, has a definite impact in fields ranging from bioimaging to nanolithography. Though the evanescent waves can be enhanced [7] or captured in the near field by sophisticated probing [8], a far-field device capable of the image forming functionality of a conventional lens, but with subwavelength resolution, would be most desirable for practical applications. The optical hyperlens [9,10] is a hollow core cylinder or half-cylinder made of materials with a strongly anisotropic dielectric response that can function as a far-field imaging device capable of resolution beyond the diffraction limit. The object to be imaged is placed inside the hollow core, and the magnified image is projected into the far field, which can be processed by conventional optics. The local wavelength at the core of the device, where the object to be imaged is placed, is below the free-space wavelength, and this leads to the subwavelength resolution. The key to achieving this wavelength compression is the hyperbolic dispersion relation in the cylindrically symmetric hyperlens, arising due to opposite signs of the dielectric permittivities in the radial ($\epsilon_r<0$) and tangential directions ($\epsilon_\theta>0$) [11]. The hyperbolic dispersion in strongly anisotropic materials implies that high wave vector (k) modes (which decay away in ordinary media such as vacuum) are supported toward the core of the hyperlens [12].

One practical realization of the cylindrically symmetric hyperlens consists of a layered medium of alternating metal and dielectric materials such that the layer thickness is significantly below the operating wavelength [1,13]. This layered structure can be described as an effective medium, yielding the desired strongly anisotropic dielectric response. In the visible spectrum, such anisotropy can be achieved by adapting existing planar metamaterial technologies in a cylindrical geometry.

The advantages of the semiclassical approach to understanding the hyperlens are twofold. First, the connection to the underlying ray optics uncovers the physical origin of light propagation and imaging in the device. Second, as opposed to brute-force numerical methods that are computationally intensive and suffer from instabilities when treating evanescent fields, the semiclassical approach, while quantitatively accurate, is both numerically inexpensive and stable. The accuracy of the semiclassical approach in the hyperlens is due to the wavelength compression in this device. As the light approaches the core of the hyperlens, the radial and tangential momentum increase due to the hyperbolic dispersion relation, leading to a substantial decrease of the wavelength.

In the present paper we formulate a Hamiltonian for a cylindrically anisotropic medium, such as the hyperlens, using the semiclassical approximation and solving for the ray dynamics. The ray trajectories reveal an interesting spiraling nature inside the device.

To verify our analytical result, we represent rays incident on the metamaterial realization of the hyperlens as a narrow Gaussian beam scattering off it and study the transmitted field in the hyperlens by solving Maxwell's equations numerically. The simulation results agree well with the semiclassical theory. The analytical equation for the ray trajectories also predicts a focusing effect for plane wave scattering from the hyperlens, which we verify numerically. Away from the spiraling regime, we use the ray trajectories to understand the beaming nature of light when a point source is placed inside the hyperlens. The parameters leading to optimum resolution can thus be identified, which is critical to subwavelength im-

aging. Finally, we note that deviations from the semiclassical picture can provide insight into the regime of validity of the effective medium approximation.

2. SEMICLASSICAL THEORY

A. Eikonal Equation of Optics for a Cylindrically Anisotropic Medium

We start with Maxwell's equations in cylindrical coordinates

$$\nabla \cdot \vec{D} = 0, \quad \nabla \cdot \vec{B} = 0, \quad \nabla \times \vec{B} = \frac{1}{c}\frac{\partial \vec{D}}{\partial t}, \quad \nabla \times \vec{E} = -\frac{1}{c}\frac{\partial \vec{B}}{\partial t}. \tag{1}$$

Using the constitutive relation $D=\epsilon E$, where ϵ is the dielectric permittivity tensor for a cylindrically anisotropic inhomogeneous medium, we get

$$\nabla \times [\epsilon^{-1}(\nabla \times \vec{B})] = \frac{\omega^2}{c^2}\vec{B}. \tag{2}$$

For fields with the magnetic field along the axis in the cylindrically symmetric hyperlens, the above equation can be simplified for the scalar function B_z,

$$\frac{1}{r}\frac{\partial}{\partial r}\left\{\frac{r}{\epsilon_\theta}\frac{\partial B_z}{\partial r}\right\} + \frac{1}{r^2}\frac{\partial}{\partial \theta}\left\{\frac{1}{\epsilon_r}\frac{\partial B_z}{\partial \theta}\right\} + \frac{\omega^2}{c^2}B_z = 0. \tag{3}$$

We now introduce the semiclassical approximation that the dielectric permittivities do not vary significantly over the local wavelength, i.e.,

$$\frac{\lambda}{r}\frac{\partial \epsilon_{ij}}{\partial \theta} \ll 1 \tag{4}$$

and

$$\lambda \frac{\partial \epsilon_{ij}}{\partial r} \ll 1. \tag{5}$$

The field can then be written as

$$B_z(r,\theta) = B_0 \exp(iS(r,\theta)), \tag{6}$$

where B_0 varies slowly on the order of wavelength but the eikonal $S(r,\theta)$ does not. Thus,

$$\frac{1}{r}\frac{\partial}{\partial r}\left\{\frac{r}{\epsilon_\theta}\frac{\partial B_z}{\partial r}\right\} \approx -\frac{1}{\epsilon_\theta}\frac{\partial^2 S}{\partial r^2}B, \tag{7}$$

$$\frac{1}{r^2}\frac{\partial}{\partial \theta}\left\{\frac{1}{\epsilon_r}\frac{\partial B_z}{\partial \theta}\right\} \approx -\frac{1}{r^2\epsilon_\theta}\frac{\partial^2 S}{\partial \theta^2}B, \tag{8}$$

where ϵ_r is the radial dielectric permittivity and ϵ_θ is the tangential dielectric permittivity. Then, in the semiclassical approximation, we can rewrite Eq. (3) as

$$\frac{1}{\epsilon_\theta}\frac{\partial^2 S}{\partial r^2} + \frac{1}{r^2\epsilon_r}\frac{\partial^2 S}{\partial \theta^2} = \frac{\omega^2}{c^2}. \tag{9}$$

Note that the time-dependant eikonal is given by

$$S_t(r,\theta) = S(r,\theta) - \omega t. \tag{10}$$

We can now write the ray optic Hamiltonian to be [14]

$$H = c\sqrt{\frac{p_r^2}{\epsilon_\theta} + \frac{p_\theta^2}{r^2\epsilon_r}}, \tag{11}$$

where c is the velocty of light in vacuum; p_r, p_θ are the radial and the angular momentum, respectively; and $\epsilon_\theta, \epsilon_r$ are the tangential and radial dielectric permittivities, respectively.

B. Ray Dynamics

Assuming constant dielectric permittivities as in the hyperlens, the equations of motion in cylindrical coordinates are

$$\dot{r} = \frac{\partial H}{\partial p_r} = \frac{c^2 p_r}{H\epsilon_\theta}, \tag{12}$$

$$\dot{\theta} = \frac{\partial H}{\partial p_\theta} = \frac{c^2 p_\theta}{H\epsilon_r r^2}, \tag{13}$$

$$\dot{p_r} = -\frac{\partial H}{\partial r} = \frac{c^2 p_\theta^2}{H\epsilon_r r^3}, \tag{14}$$

$$\dot{p_\theta} = 0, \tag{15}$$

where the last equation is just the statement of conservation of angular momentum (p_θ=const) due to the cylindrical symmetry. From the above equations we arrive at the equation of the trajectory as

$$\frac{dr}{d\theta} = \frac{\epsilon_r r^2}{\epsilon_\theta p_\theta}\sqrt{\epsilon_r \xi^2 - \frac{\epsilon_\theta p_\theta^2}{\epsilon_r r^2}}, \tag{16}$$

where $\xi=\omega/c$ is a constant of motion (ω is the frequency of the light and c is the velocity of light in vacuum). In the hyperlens we have $\epsilon_r<0$ and $\epsilon_\theta>0$, and the above equation can be analytically solved for the ray trajectory, which yields

$$r(\theta) = \frac{p_\theta}{\xi\sqrt{|\epsilon_r|}\sinh(\eta(\theta-\theta_0))}. \tag{17}$$

This is the equation of a spiral, where θ_0 is a parameter related to the initial conditions and

$$\eta = \sqrt{\frac{|\epsilon_r|}{\epsilon_\theta}} \tag{18}$$

critically determines the ray dynamics inside the hyperlens. Its implications beyond the ray approach will be presented in Subsection 5.B.

For a ray of light impinging on the hyperlens (outer radius r_{max}) from vacuum with an impact parameter ρ, we can use the conservation of angular momentum [$p_\theta = (\omega/c)\rho$] upon refraction to evaluate the constant θ_0. The above equation then becomes

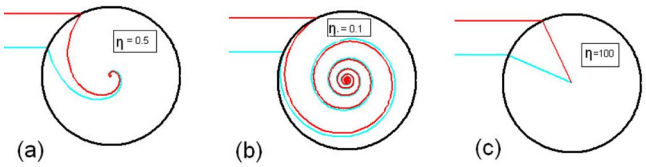

Fig. 1. (Color online) Trajectory of two rays incident on the hyperlens with different impact parameters calculated using the analytical expression (a) $\eta=0.5$ and (b) $\eta=0.1$. Note the strong spiraling behavior (c) "channeling" regime for large $\eta=100$, where rays travel in straight lines radially. Note that all rays travel toward the center.

$$r(\theta)=\frac{\rho}{\sqrt{|\epsilon_r|}\sinh(\eta(\theta-\theta_0))}, \tag{19}$$

with

$$\theta_0=\sin^{-1}\left(\frac{\rho}{r_{max}}\right)-\frac{1}{\eta}\sinh^{-1}\left(\frac{\rho}{r_{max}\sqrt{|\epsilon_r|}}\right). \tag{20}$$

We plot the analytical result in Figs. 1(a) and 1(b) for small values of the parameter η, which explicitly shows the spiraling behavior. The negative refraction of the ray is consistent with the negative refraction of the Poynting vector known in strongly anisotropic materials. For large values of the parameter η we are in the "channeling" regime [15], where the ray moves in a straight line inside the hyperlens.

3. PRACTICAL REALIZATIONS OF CYLINDRICAL ANISOTROPY: EFFECTIVE MEDIUM THEORY

There exist no natural materials with the desired cylindrical anisotropy in the dielectric response. However, the required anisotropy can be attained using metamaterials, e.g., a hollow core cylinder consisting of "slices" of metal and dielectric materials or alternating concentric layers of metal and dielectric materials (Fig. 2). The layer thickness h in each of these structures is much less than the wavelength λ, and when $h\ll\lambda\leq r$ we can use the effective medium theory to write the effective dielectric permittivity as

$$\epsilon_\theta=\frac{\epsilon_m+\epsilon_d}{2}, \tag{21}$$

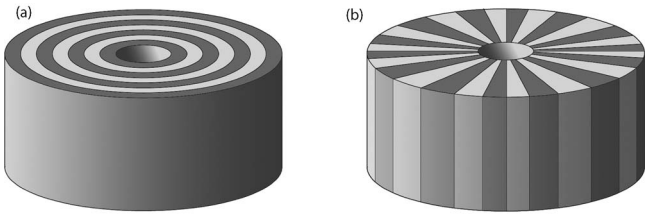

Fig. 2. Possible realizations of metacylinders. (a) Concentric alternate metallic layers and dielectric layers or (b) radially symmetric "slices" of metal and dielectric materials produce ($\epsilon_\theta>0, \epsilon_r<0$) anisotropy. This results in a hyperbolic dispersion relation necessary for penetration of the field close to the center.

$$\epsilon_r=\frac{2\epsilon_m\epsilon_d}{\epsilon_m+\epsilon_d}, \tag{22}$$

where ϵ_m and ϵ_d denote the permittivities of the metal and dielectric layers, respectively. A low-loss cylindrically anisotropic material can also be achieved by metallic inclusions in a hollow core dielectric cylinder.

It should be noted that the polar dielectric permittivities are ill-defined at the center and any practical realization of cylindrical anisotropy, such as metamaterial structures, can only closely approximate the desired dielectric permittivities away from the center (when $r\geq\lambda$). For $R_{\text{inner}}\geq\lambda$, however, as we verify from simulations, the effective medium description is adequate.

4. NUMERICAL SIMULATIONS

The hyperlens is described in the effective medium theory as a cylindrically anisotropic medium with ($\epsilon_r<0$) and ($\epsilon_\theta>0$). Near the core of the hyperlens, the effective wavelength is smaller than the free-space wavelength and the ray optics limit is approached. On the other hand, a smaller effective wavelength and larger radius of curvature near the core implies the effective medium theory presented above for any practical metamaterial realization of the hyperlens might no longer be valid. This necessitates a study of the layered hyperlens beyond the effective medium approximation.

A. Fields in the Hyperlens: beyond the Effective Medium Approximation

As mentioned in the previous section, one metamaterial realization of the hyperlens consists of a hollow core of radius r_{min} surrounded by N alternating layers of metal ($\epsilon_m<0$) and dielectric ($\epsilon_d>0$) materials. The outer radius is denoted by r_{max}, and the thickness of each layer h is much less than the wavelength λ. For fields with the magnetic field B_z along the axis of the hyperlens [16],

$$B_z=R_1(r)\exp(im\theta), \tag{23}$$

where $R_1(r)$ satisfies the Bessel equation in the cylindrical layers,

$$r^2\frac{d^2R_1}{dr^2}+r\frac{dR_1}{dr}+[\epsilon_i k^2r^2-m^2]R_1=0, \tag{24}$$

and $\epsilon_i=\epsilon_m$ or ϵ_d depending on whether the field is being evaluated in the metal layer or dielectric layer; m is the angular momentum number. Any field inside the hyperlens can be expressed on the basis of such angular momentum modes. The radial function is written as a linear

combination of two functions f_1 and f_2, which satisfy the Bessel equation

$$R_1(r) \equiv c_1 f_1(\sqrt{|\epsilon_i|}k_0 r) + c_2 f_2(\sqrt{|\epsilon_i|}k_0 r), \tag{25}$$

where c_1 and c_2 are constants. In the dielectric layer, the functions (f_1, f_2) are the ordinary Bessel functions (J_m, Y_m), and in the metal layer, the functions (f_1, f_2) can be taken to be the modified Bessel functions (I_m, K_m). At times it is convenient to express the fields on the basis (f_1, f_2) that is itself a linear combination of the Bessel functions, such as the Hankel functions (H_m^+, H_m^-), where the superscript denotes incoming (−) or outgoing (+) cylindrical waves

B. Gaussian Beam Scattering from the Hyperlens

We represent a pencil of rays incident on the hyperlens as a narrow Gaussian beam scattering from it and study the transmitted field by solving Maxwell's equations numerically. The center of the Gaussian beam moves along the ray of light as shown in Fig. 3. We express the TM-polarized monochromatic Gaussian beam on the basis of angular momentum modes as

$$B_y^{inc}(x,z) = \sum_{m=-\infty}^{m=\infty} i^m J_m(kr)\exp(im\phi)A_m, \tag{26}$$

where, for a Gaussian beam,

$$A_m = \int_{-\infty}^{\infty} e^{-k_x^2/(2\sigma_k)^2 + ix_0k_x + iz_0k_z + im\alpha} dk_x, \tag{27}$$

where $J_m(kr)$ denotes the Bessel function of the first kind; m is the angular momentum mode number; (r, ϕ) are the polar coordinates of the point P with Cartesian coordinates (x,z); k_x and k_z are the components of the wave vector k along the x and z axes, respectively; $(-x_0, -z_0)$ are the coordinates of the center of the Gaussian beam where the width is a minimum; α is the angle the wave vector makes with the z axis; and σ_k is the width of the Gaussian beam in k-space. At the point of impact (impact parameter $p = x_0$), part of the Gaussian beam will be reflected and part of it will be transmitted.

The scattered part of the beam can be written as a superposition of outgoing cylindrical waves only [14]:

$$B_y^{scatt}(x,z) = \sum_{m=-\infty}^{m=\infty} i^m (r_m - 1) H_m^{(1)}(kr)\exp(im\phi)A_m, \tag{28}$$

where $H_m^1(kr)$ is the Hankel function of the first kind, which represents the radial part of an outgoing cylindrical wave of angular momentum mode m, and r_m is the reflection coefficient for the mth angular momentum mode incident on the hyperlens. The field outside the hyperlens can be be written as the sum of the incident field and the scattered field,

$$B_y^{outer}(x,z) = B_y^{inc}(x,z) + B_y^{scatt}(x,z). \tag{29}$$

The field in the jth layer with permittivity ϵ_j can be written on the basis of incoming and outgoing cylindrical waves as

$$B_y^j(x,z) = \sum_{m=-\infty}^{m=\infty} [\gamma_m H_m^{(1)}(\sqrt{\epsilon_j}kr)\exp(im\phi) + \delta_m H_m^{(2)}(\sqrt{\epsilon_j}kr)\exp(im\phi)], \tag{30}$$

and the field in the core is

$$B_y^{core}(x,z) = \sum_{m=-\infty}^{m=\infty} [\mu_m J_m(kr)\exp(im\phi)]. \tag{31}$$

Note that the Hankel functions $H_m^{(1),(2)}$ diverge at the center, and hence the field in the core where $0 \leq r \leq r_{min}$ is expressed only in terms of the Bessel functions of the first kind. For the TM mode, B_y and $\epsilon^{-1}\partial B_y/\partial r$ are continuous across an interface and the constants γ_m, δ_m, and μ_m can be evaluated by matching boundary conditions on the appropriate interfaces. The numerical procedure to evaluate the fields has to be chosen wisely due to the large number of layers, their subwavelength nature, and also the presence of metallic layers, which cause exponential variation of the field. The knowledge of the angular momentum mode penetration within the caustic as expected from the effective medium theory is crucial to making the solution converge with sufficient accuracy [9].

5. RESULTS AND DISCUSSION

A. Gaussian Beam Scattering

If we visualize a Gaussian beam impinging on the layered hyperlens with impact parameter p [Fig. 3(a)] as a pencil of parallel rays, then Eq. (19) predicts that the distance between the rays will decrease as it approaches the core, where they bounce off the inner hollow region. This is seen by plotting the analytical expression inside the hyperlens for $(\eta = 1, \epsilon_\theta = 1, \epsilon_r = -1)$ and considering specular reflection at the inner radius [Fig. 3(b)]. By choosing an appropriate metal $(\epsilon_m \approx -0.4)$ and dielectric material $(\epsilon_d \approx 2.4)$, we can achieve the layered hyperlens yielding the desired dielectric response, which is $\epsilon_\theta = 1, \epsilon_r = -1$ accord-

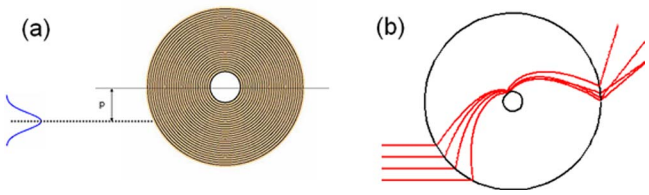

Fig. 3. (Color online) (a) Schematic of a Gaussian beam with impact parameter p impinging on the layered hyperlens (top view), consisting of alternate layers of metal and dielectric materials. The inner hollow region and region outside the hyperlens are vacuum. (b) Ray trajectories representing the Gaussian beam calculated for the effective medium parameters (Section 3) of the hyperlens using Eq. (19). Note the narrowing of the Gaussian beam, predicted by the semiclassical theory, toward the core of the hyperlens. We consider specular reflection at the inner core.

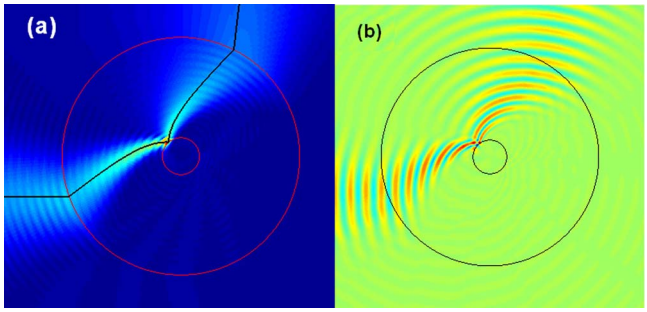

Fig. 4. (Color online) (a) Absolute value of the field shown in false color for a Gaussian beam scattering from the layered hyperlens with parameters $p \sim 4\lambda$, $r_{min} \sim \lambda$, $r_{max} \sim 7\lambda$, $h \sim \lambda/100$, $\epsilon_m \sim -0.4$, $\epsilon_d \sim 2.4$. The inner and outer boundaries of the hyperlens are shown in red (online). The ray trajectory shown in black is calculated using Eq. (19) and specular reflection at the inner boundary. Note the narrowing of the Gaussian beam and also that the center of the beam moves along the calculated ray trajectory. (b) Real part of the field due to Gaussian beam scattering. The negative refraction of the Poynting vector, which is along the direction of the beam, is clearly seen. The wave vector (k) refracts positively, as can be seen by drawing the normal to the phase fronts.

ing to Eqs. (23) and (24). We choose an inner radius of λ, outer radius 7λ, thickness of layers $\lambda/100$, $N=600$ layers, and impact parameter $p=2.4\lambda$ at an operating wavelength of 700 nm.

The magnitude of the field is plotted in false color in Fig. 4(a), and the ray trajectory calculated from Eq. (19) is shown in black superimposed on the field plot. Blue denotes regions of low intensity, and red denotes regions of high intensity (color online). The two circles denote the inner and outer boundaries of the device. The ray is clearly seen to move along the center of the Gaussian beam. The narrowing effect obtained from the ray equations [Fig. 3(b)] is evident in the width of the Gaussian beam near the core [Fig. 4(a)]. This validates the semiclassical description presented and also the adequacy of the effective medium approximation in describing the hyperlens.

In Fig. 4(b) we plot the real part of the field in false color. Green corresponds to regions of zero intensity, and red corresponds to regions of maximum intensity (color online). In this case, the direction of energy flow (Poynting vector or ray) is the direction of group velocity, which is nothing but the direction of propagation of the Gaussian beam itself. It can be verified from the ray dynamical equations in Subsection 2.B that the direction of motion of the ray is along the Poynting vector as expected in an anisotropic medium. The wave vector is given by the normal to the phase fronts. The negative refraction of the Poynting vector and the positive refraction of the wave vector, as expected, on impact with the hyperlens are clearly seen.

For lower values of η we have strong spiraling behavior of rays in the hyperlens (Fig. 5). We now consider a metamaterial hyperlens with $N=420$ layers of appropriate metal and dielectric materials, each of thickness $\lambda/70$ such that the effective medium theory gives $\epsilon_\theta \approx 1$ and $\epsilon_r \approx -0.01$ ($\eta=0.1$). Note that the choice of ($\epsilon_\theta \approx 1$) helps to minimize reflections and get maximum light into the device. The trajectory obtained by the analytical result using effective medium parameters is shown in the inset of Fig. 5. The spiraling Gaussian beam field obtained by solving Maxwell's equations numerically is shown in false color (online) in Fig. 5.

We now look at a case where the semiclassical result differs from the numerical simulations. The deviation of the center of the Gaussian beam from the analytical result for rays can be seen in Fig. 6, where we consider a metamaterial hyperlens of the same parameters but thicker layers ($h \approx \lambda/20$). The point of impact at the inner

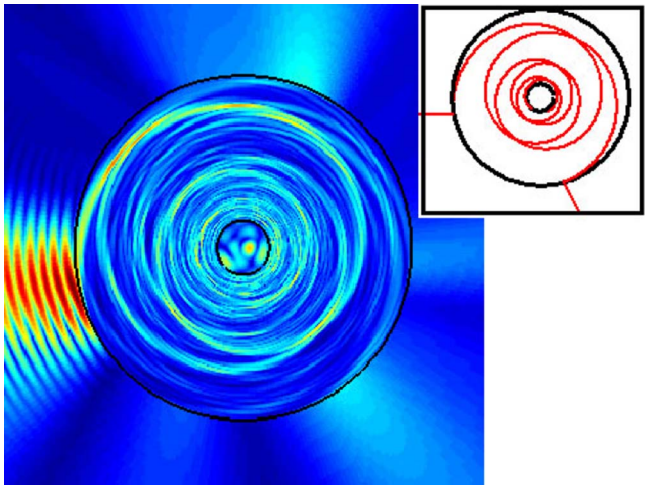

Fig. 5. (Color online) Strong spiraling behavior for a Gaussian beam incident ($p \sim 1.4\lambda$) on the layered hyperlens with $r_{min} \sim \lambda$, $r_{max} \sim 7\lambda$, and $h \sim \lambda/70$ and metal and dielectric materials chosen to achieve $\epsilon_\theta \approx 1$ and $\epsilon_r = -0.01$. The magnitude of the field is shown in false color (online), while the trajectory predicted by the semiclassical theory is plotted in the inset.

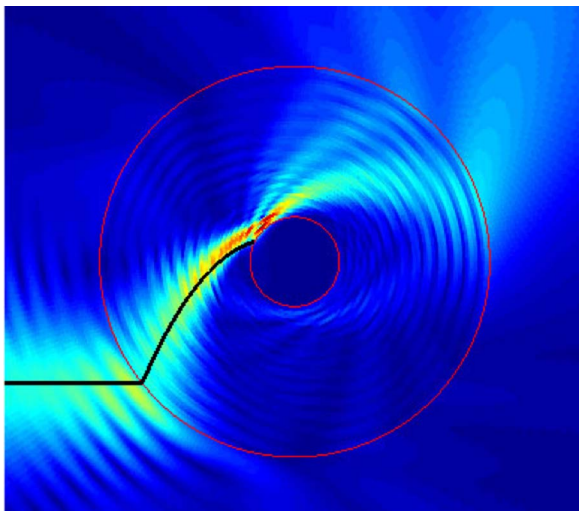

Fig. 6. (Color online) Deviations from effective medium theory for thick layers. Near the core, the trajectory obtained by Eq. (19) (shown in black) does not match the numerical field calculations obtained by Gaussian beam scattering.

region for the Gaussian beam and the ray (shown in black) is different even though initially the center of the Gaussian beam and ray trajectory match closely. This shows that the effective medium approximation does not hold close to the core for thick layers. The compression of wavelength means the desired dielectric response deviates from $\epsilon_\theta=1$ and $\epsilon_r=-1$ toward the core unless the layer thicknesses are chosen appropriately. Note that for a slight deviation, the qualitative behavior of spiraling rays and Gaussian beam narrowing still remains the same.

B. Semiclassical Description of Imaging in the Hyperlens

Due to the wavelength compression in the hyperlens, the intuitive ray optics approach yields results consistent with full solutions of Maxwell's equations even though the size of the device is comparable to the vacuum wavelength. The imaging characteristics are best understood by considering the case of two point sources separated by a distance below the diffraction limit and kept in the hollow core of the hyperlens very close to its boundary. We first note that a point source kept in an isotropic medium such as vacuum radiates uniformly in all directions. The field of the point source can be written as a superposition of plane waves. The allowed values of the wave vectors of the constituent plane waves are just the vectors from the origin to points on the dispersion curve [solid red (color online) arrows in Figs. 7(a) and 7(b)]. The dispersion curve is a circle in the case of isotropic media such as vacuum [Fig. 7(a)]. The normal to the dispersion curve at these points gives the direction of the Poynting vector for each of these plane waves [dashed red (color online) arrows in Figs. 7(a) and 7(b)]. The rays of light are in the direction of these Poynting vectors. In the case of an isotropic medium, the Poynting vector is in the direction of the wave vector, and energy is carried away in all directions by the plane waves. In contrast, a strongly anisotropic medium, which has a hyperbolic dispersion curve, allows real wave vectors only in certain directions [Fig. 7(b)]. All the real wave vectors lie within the region bounded by the asymptotes of the hyperbola. These asymptotes pass through the origin and are tangent to the dispersion curve at infinity [black dashed lines in Fig. 7(b)]. There are wave vectors along the asymptote that correspond to the points on the hyperbola at infinity.

In the case of no losses, note that there are infinitely many wave vectors accumulated close to the asymptotes of the hyperbola. The Poynting vectors corresponding to these wave vectors all point in the same direction, perpendicular to the asymptote. The direction of the Poynting vector, which in this case is not the same as the wave vector, can be found by drawing the normal to the dispersion relation [Fig. 7(b)]. The inward or outward normal is determined by calculating from Maxwell's equations whether the angle between the Poynting vector and the wave vector is acute or obtuse. Since the real wave vectors lie within the region bounded by the asymptotes, the Poynting vectors will lie within the region bounded by the

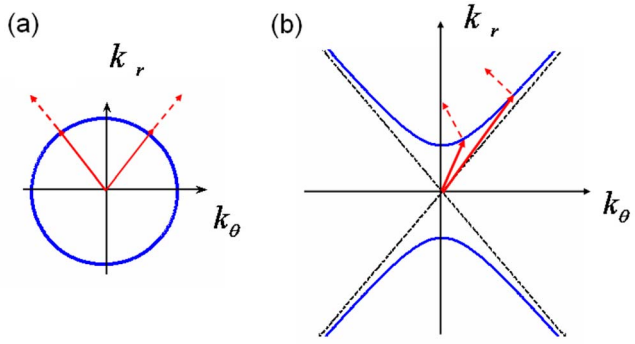

Fig. 7. (Color online) Dispersion relations (curves), wave vectors (solid arrows), Poynting vectors, and ray directions (dashed arrows). (a) Circular dispersion relation for an isotropic medium. The Poynting vectors are parallel to the respective wave vectors drawn from the origin to various points on the curve; hence a point source radiates isotropically. (b) Hyperbolic dispersion relation for a strongly anisotropic medium. The Poynting vector is not parallel to the wave vector, and they lie within a cone whose half-angle is related to the angle between the asymptotes of the hyperbola (dashed lines), leading to a beamlike point source radiation pattern.

normal to these asymptotes. The energy is carried away by the plane waves only within this "conical" region bounded by the two extreme Poynting vectors. The extremal Poynting vectors are perpendicular to the two asymptotes. This gives rise to the beamlike radiation pattern of a point source kept in a strongly anisotropic medium. These directional radiation patterns are known as resonance cones [17] and were studied in relation to sources in strongly anisotropic plasmas [18]. The beam divergence angle is related to the angle between the asymptotes of the hyperbola.

$$\tan(\theta_c) = \sqrt{\frac{\epsilon_\theta}{|\epsilon_r|}} = \frac{1}{\eta}, \tag{32}$$

where θ_c is the extremal angle of the Poynting vector cone and η is the parameter that enters in the semiclassical equation determining the spiraling or "channeling" regime. For large values of η, the cone angle tends to zero, while the angle between the asymptotes becomes large and radiation from a point source takes place in a narrow beamlike pattern. This is precisely the condition for subdiffraction imaging. We note from Fig. 1(c) that in the "channeling" regime, rays of light move in the hyperlens in straight lines, which is essential for a narrow beam divergence angle.

We verify this fact using the analytical expression for rays inside the hyperlens in the case of two point sources kept inside the hyperlens. The point source is represented as a source of rays in all directions, as shown in the inset of Fig. 8(a). Note that even though we have assumed isotropic emission in the core, the density of rays is high within two conelike regions within the hyperlens. The rays of light are negatively refracted at the inner curved surface of the hyperlens, which helps in the formation of a beam. Inside the hyperlens, the rays then move in straight lines, almost radially, traveling to the outer interface. These rays arrive at normal incidence and the beamlike nature in the hyperlens is preserved while emerging into vacuum. Thus the two point sources give rise to two distinct beams in the far field even though they are separated below the diffraction limit inside the hyperlens. Furthermore, due to the cylindrical geometry and almost radial nature of propagation, the distance between the point sources is magnified to the scale beyond the diffraction limit.

We verify this behavior by considering a practical realization of the hyperlens mentioned in Section 3 made of alternating layers of metal ($\epsilon_m \approx -1$) and dielectric ($\epsilon_d \approx 1.1$) materials to achieve a dielectric response in the effective medium approximation ($\epsilon_\theta = 0.05$) and ($\epsilon_r = -22$). This gives a value of $\eta \approx 20$, which is large, and hence we are in the "channeling" regime. The magnification due to the radial nature of light propagation is the ratio of the radii, which is ≈ 5 in our case. We solve Maxwell's equations numerically in this system, and the absolute value of the field is shown in false color (online) where the high intensity corresponds to red and low intensity corresponds to blue (color online). The two beams emanating from the point sources that carry information to the far field can clearly be seen in Fig. 8(b), consistent with the plot obtained by the analytical expression for rays in the hyperlens. It should be noted that the effective medium approximation is thus accurate in describing the practical realization of the hyperlens.

C. Plane Wave Scattering

The effect of plane wave scattering on the hyperlens in the spiraling regime is also interesting as predicted by the ray dynamics presented in Section 1. We consider parallel rays impinging on the hyperlens simultaneously with various impact parameters. For small values of η we see that the rays intersect inside the hyperlens and then bounce off the inner hollow core of the hyperlens (we consider specular reflection) and proceed in a beamlike fashion out of the hyperlens. These parallel rays present the effect of plane wave scattering from the hyperlens. Following the procedure presented in Section 3, but considering $A_m = 1$ for each angular momentum mode, we get the expansion of the plane wave on a cylindrical basis. The fields can then be evaluated in and around the hyperlens numerically due to plane wave scattering. The results are shown for the layered hyperlens of outer radius 5λ, inner radius λ, effective tangential permittivity 1, and effective radial permittivity −1.

The focusing effect, as well as beamlike exit from the

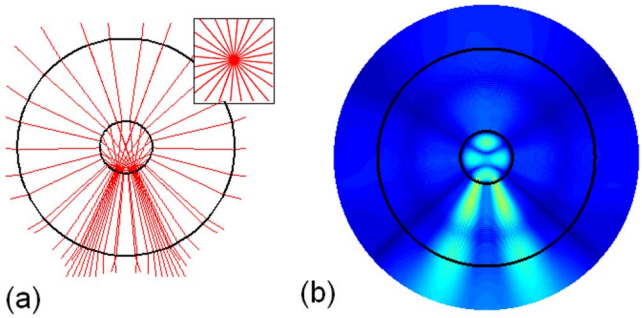

Fig. 8. (Color online) Subdifraction imaging in the hyperlens. (a) Beamlike radiation obtained from Eq. (19) for two point sources kept near the inner boundary of the hyperlens for large η ("channeling" regime). The rays are negatively refracted at the inner surface and proceed radially outward, leading to magnification at the outer surface. The point source is represented as a source of rays in all directions (inset). (b) Numerical confirmation of the beamlike radiation using a layered metamaterial hyperlens made of alternating layers of metal ($\epsilon_m \approx -1$) and dielectric ($\epsilon_d \approx 1.1$) materials and two point sources near the inner boundary. The magnitude of the field is shown in false color.

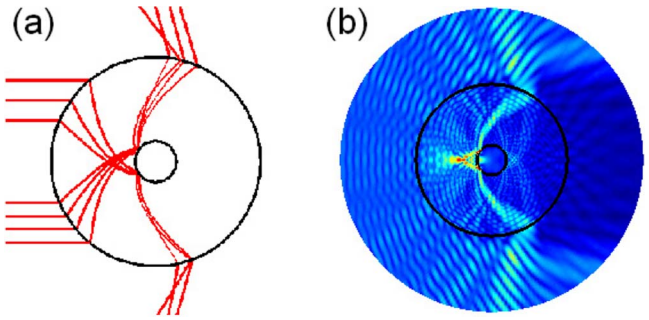

Fig. 9. (Color online) (a) Parallel rays incident on the hyperlens in the spiraling regime intersect inside the hyperlens, bounce off the inner region, and proceed in a beamlike nature. This implies plane wave scattering from the hyperlens should show a focusing effect. (b) Numerical verification of the focusing effect for a layered hyperlens ($r_{min} \sim \lambda$, $r_{max} \sim 5\lambda$, $h \sim \lambda/60$, $\epsilon_m \sim -0.4$, $\epsilon_d \sim 2.4$) realization. The boundaries of the hyperlens are shown by dark circles.

hyperlens, is clearly visible in the plot of the intensity shown in false color (online) in Fig. 9.

6. CONCLUSION

We have presented the semiclassical theory of the hyperlens, an imaging device with subwavelength far-field resolution capabilities. The obtained analytical result explains imaging behavior of the device as well as predicts other interesting effects such as spiraling rays and focusing of incident plane waves. The numerical solution of Maxwell's equations in a metamaterial realization of the hyperlens shows good agreement with the analytical results. The validity of the ray optics approach is due to the wavelength compression in the device.

ACKNOWLEDGMENTS

This work was partially supported by National Science Foundation grants DMR-0134736 and ECS-0400615, by Army Research Office–Multidisciplinary Research Program of the University Research Initiative (ARO-MURI), and by Princeton Institute for the Science and Technology of Materials (PRISM).

REFERENCES

1. Z. Liu, H. Lee, Y. Xiong, C. Sun, and X. Zhang, "Far-field optical hyperlens magnifying sub-diffraction-limited objects," Science **315**, 1686 (2007).
2. R. A. Shelby, D. R. Smith, and S. Schultz, "Experimental verification of a negative index of refraction," Science **292**, 77–79 (2001).
3. V. M. Shalaev, W. Cai, U. K. Chettiar, H.-K. Yuan, A. K. Sarychev, V. P. Drachev, and A. V. Kildishev, "Negative index of refraction in optical metamaterials," Opt. Lett. **30**, 3356–3358 (2005).
4. N. Fang, D. Xi, J. Xu, M. Ambati, W. Srituravanich, C. Sun, and X. Zhang, "Ultrasonic metamaterials with negative modulus," Nat. Mater. **5**, 452–456 (2006).
5. V. G. Veselago, "The electrodynamics of substances with simultaneously negative values of permittivity and permeability," Sov. Phys. Usp. **10**, 509 (1968).
6. J. B. Pendry, "Negative refraction makes a perfect lens," Phys. Rev. Lett. **85**, 3966–3969 (2000).
7. N. Fang, H. Lee, C. Sun, and X. Zhang, "Sub-diffraction-limited optical imaging with a sliver superlens," Science **308**, 534–537 (2005).
8. B. Hecht, B. Sick, U. P. Wild, V. Deckert, R. Zenobi, O. J. F. Martin, and D. W. Pohl, "Scanning near-field optical microscopy with aperture probes: fundamentals and applications," J. Chem. Phys. **112**, 7761 (2000).
9. Z. Jacob, L. V. Alekseyev, and E. Narimanov, "Optical hyperlens: far-field imaging beyond the diffraction limit," Opt. Express **14**, 8247–8256 (2006).
10. A. Salandrino and N. Engheta, "Far-field subdiffraction optical microscopy using metamaterial crystals: theory and simulations," Phys. Rev. B **74**, 075103 (2006).
11. V. A. Podolskiy and E. E. Narimanov, "Strongly anisotropic waveguide as a nonmagnetic left-handed system," Phys. Rev. B **71**, 201101 (2005).
12. A. A. Govyadinov and V. A. Podolskiy, "Meta-material photonic funnels for subdiffraction light compression and propagation," Phys. Rev. B **73**, 155108 (2006).
13. I. Smolyaninov, Y. Hung, and C. Davis, "Magnifying superlens in the visible frequency range," Science **315**, 1699–1701 (2007).
14. L. D. Landau, E. M. Lifshitz, and L. P. Pitaevskii, *Course of Theoretical Physics*, 2nd ed. (Reed Ltd., 1984).
15. P. A. Belov, C. R. Simovski, and P. Ikonen, "Canalization of subwavelength images by electromagnetic crystals," Phys. Rev. B **71**, 193105 (2005).
16. M. A. Kaliteevski, R. A. Abram, V. V. Nikolaev, and G. S. Sokolovski, "Bragg reflectors for cylindrical waves," J. Mod. Opt. **46**(5), 875–890 (1999).
17. R. K. Fisher and R. W. Gould, "Resonance cones in the field pattern of a short antenna in an anisotropic plasma," Phys. Rev. Lett. **22**, 1093–1095 (1969).
18. E. Arbel and L. B. Felsen, "Theory of radiation from sources in anisotropic media," in *Electromagnetic Theory and Antennas*, E. C. Jordan, ed. (Pergamon, 1963), pp. 391–421.